Langmuir

ARTICLE

pubs.acs.org/Langmuir

Surface Nanobubbles as a Function of Gas Type

Michiel A. J. van Limbeek and James R. T. Seddon*

Physics of Fluids, MESA+ Institute for Nanotechnology, University of Twente, P.O. Box 217, 7500 AE Enschede, The Netherlands

ABSTRACT: We experimentally investigate the nucleation of surface nanobubbles on PFDTS-coated silicon as a function of the specific gas dissolved in water. In each case, we restrict ourselves to equilibrium conditions (c = 100%, T_{liquid} = $T_{substrate}$). Not only is nanobubble nucleation a strong function of gas type, but there also exists an optimal system temperature of ∼35 −40 °C where nucleation is maximized, which is weakly dependent on gas type. We also find that the contact angle is a function of the nanobubble radius of curvature for all gas types investigated. Fitting this data allows us to describe a line tension that is dependent on the type of gas, indicating that the nanobubbles sit on top of adsorbed gas molecules. The average line tension was $\tau \approx -0.8$ nN.

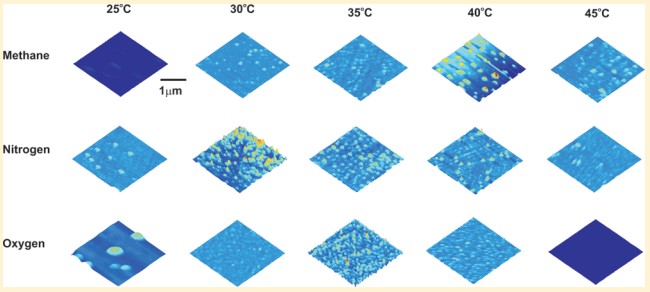

INTRODUCTION

Surface nanobubbles are nanoscopic gaseous domains that exist on the solid/liquid interface.[1−11] They are surprisingly stable,[10,12−14] surviving orders of magnitude longer than the classical diffusive lifetime. Since their recent discovery, several key observations have been made regarding the ideal conditions for nucleation.[15−17] These include the (almost[18,19]) uniqueness for formation in water or in solutions containing at least some part water. However, changing the substrate chemistry can lead to differences in the typical nanobubble sizes and distributions,[6,20−22] but nanobubbles are always found as long as sufficient care is used as well as an appropriate experimental technique/pretreatment.[2−4,6,23−26]

One area that has seemingly escaped detailed research is the dependence of nanobubble formation on the type of gas that is dissolved in water. Almost all studies to date investigate nanobubbles made from "air", with the few exceptions including carbon dioxide,[12,16,27] butane,[26,28] and nitrogen.[26] (We omit here the hydrogen and oxygen nanobubbles created using electrolysis[29−31] because gas was not necessarily dissolved in the water.) Of these specific gases, carbon dioxide and butane seem to be peculiar choices. Both of these gases have triple points above room temperature, so they can liquefy if the pressure is high enough (i.e., if they fill a nanobubble that is small enough). As an example, carbon dioxide was used as a reference[12] because of its strong rotational fine structure signal, which allowed the use of the attenuated total reflection infrared spectroscopy technique to show conclusively that nanobubbles contain gas. However, the critical pressure and temperature of CO_2 are p_c = 7.4 MPa and T_c = 31.0 °C,[32] respectively, so we would expect liquefaction to occur in these CO_2-filled nanobubbles if their radii of curvature was lower than $R_c = 2\gamma/(p_c - p_0) \approx 20$ nm. (Note that the nanobubbles in ref 12 were much larger than this.) In butane-saturated water, nanodroplets have already been reported on Si(100) by Kameda et al.[21]

It is clear that gas type plays an important role, but no study has ever been carried out to investigate the effects of different gases. Thus, we have directly investigated the role of gas type on the formation of surface nanobubbles. We chose a selection of different gases, including noble gases (helium and argon), diatomic gases (hydrogen, nitrogen, and oxygen), and more complex gases (carbon dioxide and methane). Furthermore, for each gas type we restricted ourselves to systems where the liquid was saturated with the gas and specifically not supersaturated, following recent observations that supersaturation is not a requirement for nanobubble formation.[17] Thus, our observations provide information on surface nanobubble nucleation in equilibrium.

EXPERIMENTAL METHOD

The substrate was a silicon wafer that had been hydrophobized with a self-assembled monolayer of perfluorodecyltrichlorosilane (PFDTS), following the guidelines in refs 33 and 34. In brief, we degassed the chamber that contained the uncoated substrate to a pressure of ∼50 μbar (i.e., below the vapor pressure of the PFDTS). Next, we opened this chamber to a reservoir of degassed PFDTS for 5 min so that the silane molecules adsorbed onto the substrate. Finally, we closed the system off to the PFDTS reservoir and opened it to a reservoir of degassed pure water for half an hour, hence increasing the pressure of the system to the vapor pressure of water to allow the reagents to react. The resulting rms roughness was 0.4 nm, and the contact angles were ∼110° (equilibrium), ∼116° (advancing), and ∼104° (receding). This surface has no known phase transitions in the temperature range investigated in the present study.

The substrate was mounted on a temperature-controlled sample plate (331 temperature controller, Lakeshore, U.S.) before a purpose-built

Received: February 11, 2011
Revised: May 28, 2011
Published: June 16, 2011

atomic force microscope (AFM) liquid cell was firmly mounted on top. The AFM was an Agilent 5100 operating in tapping mode with a typical scan speed of 4 to 5 μm/s. The AFM cantilevers were hydrophilic, Au-back-coated Si_3N_4 Veeco NPG probes with typical spring constants and resonance frequencies in water of 0.58 N/m and 25−35 kHz. We operated the AFM at a set point of 90%.

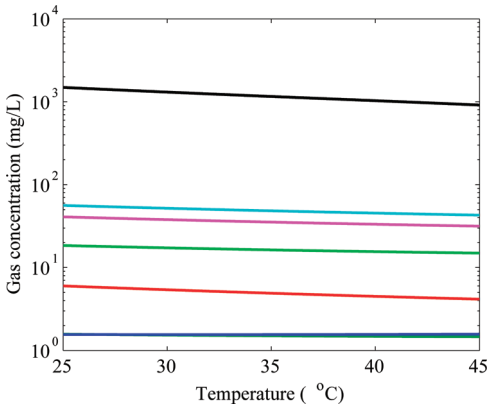

Figure 1. Concentration of saturated gases in water as a function of temperature. Colors are for H_2 (dark green), He (blue), CH_4 (red), N_2 (green), O_2 (magenta), Ar (cyan), and CO_2 (black). Note that the data for H_2 and He overlap each other.

For the liquid, we used ultrapure water (Simplicity 185 purification system, Millipore SAS, France). This was placed within a stainless steel container that included a pump-out port, a repressurization port, and a digital pressure gauge.

Our study was to investigate the role of the gas type on nanobubble nucleation, so we now explain the procedure that we used to prepare the gas dissolved in the water. The first stage of preparation was to degas the water thoroughly to remove as much air as possible. During this stage, the pressure was reduced to $\lesssim$20 mbar, and once this pressure was reached, we continued to pump for at least another ~30 min. The container of water was then closed off to the pump and placed within a heat bath that was at the correct temperature for the experiment at hand.

The stainless steel container had a volume of 100 mL, but we treated only 40 mL of water at a time. This allowed us to repressurise the evacuated volume above the water level with a specific type of gas. The number of molecules of a specific type that dissolve in water at equilibrium is well known,[32] thus the magnitude of the repressurization was 1 atm plus the required number of molecules for dissolution multiplied by kT/V_w, where kT is the thermal energy and V_w is the 40 mL volume of water. We plot the solubilities of the different gases used in this study, as functions of temperature, in Figure 1. After the

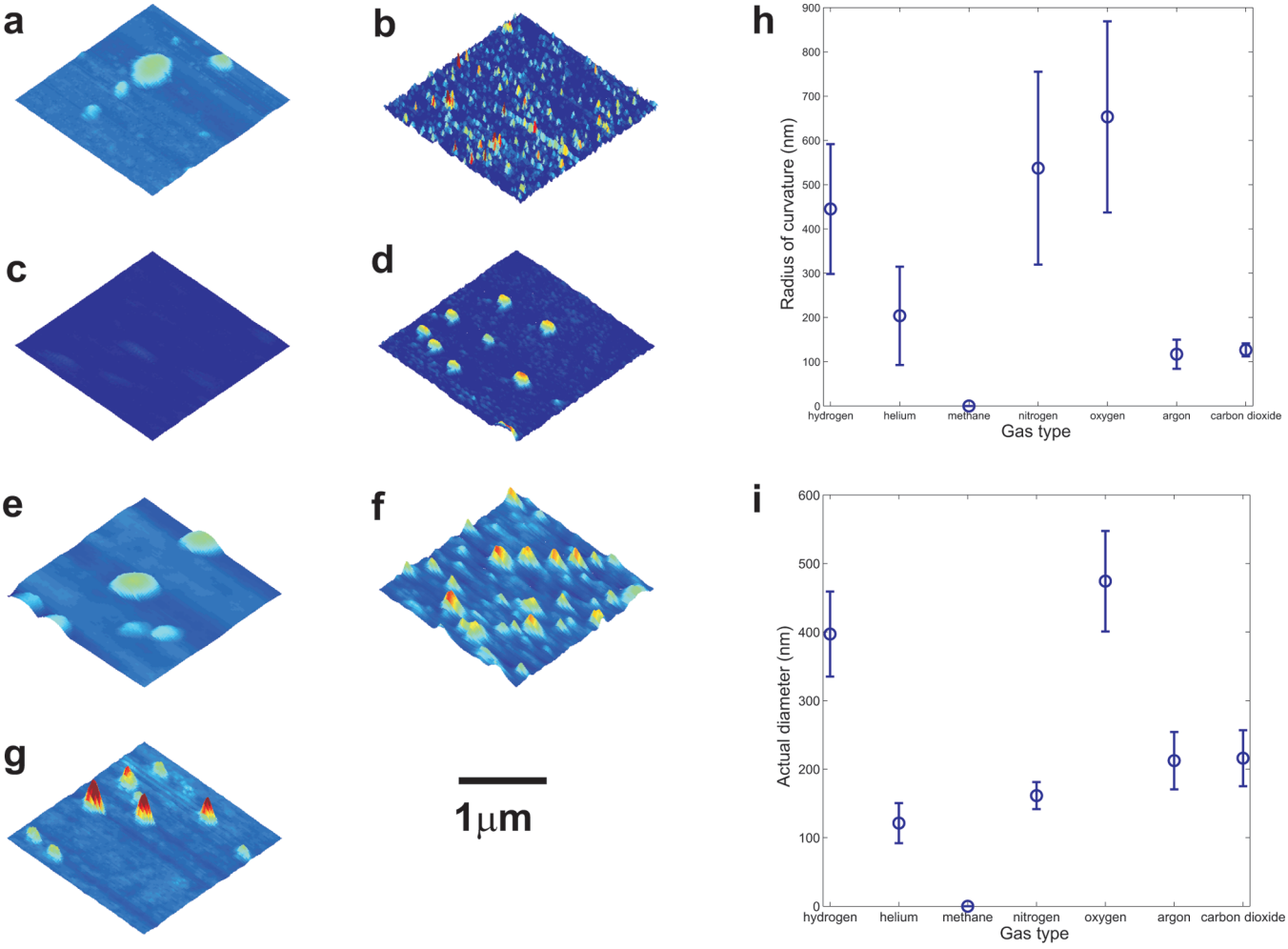

Figure 2. Typical images of nanobubbles formed from different gas types at 25 °C. Gases are (a) H_2, (b) He, (c) CH_4, (d) N_2, (e) O_2, (f) Ar, and (g) CO_2. Images are 2 μm × 2 μm; height scales are (b, d) 20 nm and (a, c, e−g) 250 nm. (h) Average radii of curvature and (i) average diameters of nanobubbles versus gas type (error bars correspond to one standard deviation).

dx.doi.org/10.1021/la2005387 |*Langmuir* 2011, 27, 8694–8699

container had been pressurized, we closed it off to the gas supply and maintained the system's seal for two to three gas-diffusion timescales.

Once the liquid was prepared, it was injected into the liquid cell of our atomic force microscope using a syringe pump. The syringe was at the same temperature as both the water and the substrate. Finally, the AFM was placed inside a glass environment control chamber that had had its air displaced with one atmosphere of the same gas type that was dissolved in the liquid. Thus, any gas exchange between the liquid and the environment would not lead to cross contamination of the gas type. This means that the gas content of the water was maintained throughout the measurements, and our results provide information about nanobubble nucleation in fully equilibrated systems.

RESULTS AND DISCUSSION

We present typical images of nanobubbles nucleated from different gases at 25 °C in Figure 2. Each image represents 2 μm × 2 μm, but the height scales differ as described in the caption. Each gas type resulted in distinct nanobubble sizes/densities, with methane being the only gas that led to zero nucleation at this temperature. Note that each set of experimental conditions was repeated in its entirety, including the water preparation stage, and for a given experiment, several areas of the substrate were scanned.

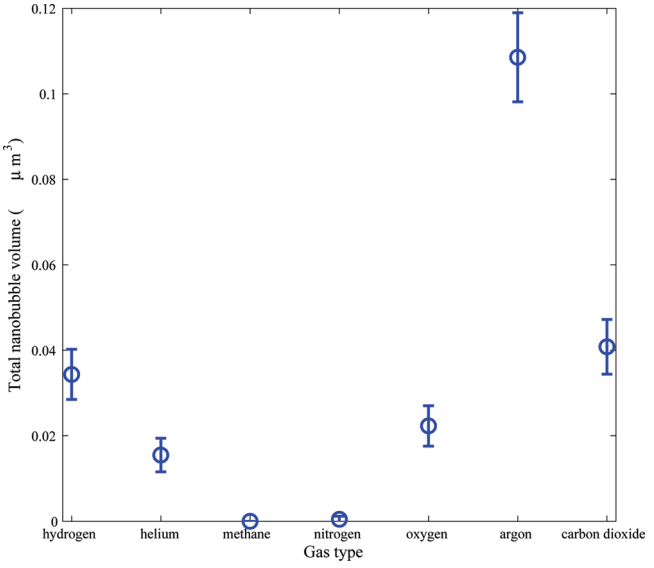

Figure 3. Total nanobubble volume on a 2 μm × 2 μm area as a function of gas type at a system temperature of 25 °C. The abscissa is ordered with increasing molecular weight and solubility. If gas solubility was the control parameter governing nucleation, then we would expect the data in this graph to vary monotonically.

To quantify the differences between gas types, we plot the average radii of curvature and diameters of nanobubbles as functions of gas type in Figure 2h,i, respectively, as well as the calculated total volume of nanobubbles on a 2 μm × 2 μm area in Figure 3, where we plot the gas type along the abscissa in order of increasing molecular weight and solubility. (Note that each data point is an average of several different areas and several experimental runs. We are displaying the average value as a standard measure of nanobubble populations. See refs 17 and 35.) If solubility was the control parameter governing nanobubble nucleation, then we would expect the data in Figure 3 to be a monotonically varying function. Clearly this is not the case, with no obvious functional form able to describe the data. This means that solubility is not the governing factor for nanobubble nucleation in a system that is in equilibrium (i.e., with the substrate and liquid temperatures being equal and the gas saturated within the liquid.)

Second, although adsorption strengths of the various gases are not known for our substrate, we expect the ordering of these to be He and H_2 (weak); Ar, O_2, and N_2 (medium); and CH_4 and CO_2 (strong).[36−38] Clearly there is no direct dependence on this either. Hence, we can rule out the possibility of nanobubbles solely nucleating from the bulk desorption of dense adsorbates, which may exist in the form of micropancakes.[34]

Another possible origin of the nucleation may be the excess gas that swells the density-depleted layer immediately next to an immersed hydrophobic solid.[39,40] However, the dependency of the amount of swelling on the gas type is currently disputed.[39,41,42] Thus, none of the three most likely possible causes of nanobubble nucleation, namely, formation from gas dissolved in the bulk, formation from molecules adsorbed on the substrate, and formation from the gas-enriched layer near the hydrophobic substrate, can be individually responsible.

To try to understand the gas dependency of nanobubble nucleation further, we proceeded to investigate the effects of

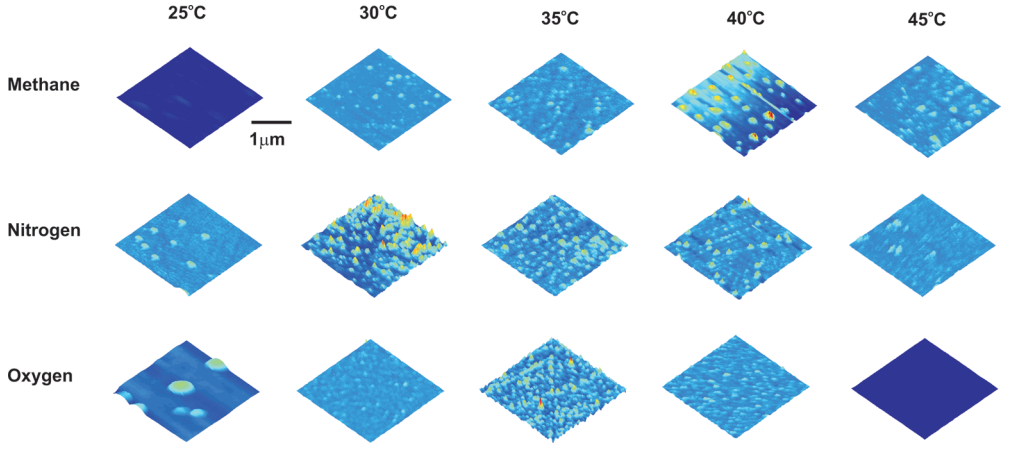

Figure 4. Temperature dependence of nanobubbles formed from methane-, nitrogen-, and oxygen-saturated water at temperatures of (a) 25, (b) 30, (c) 35, (d) 40, and (e) 45 °C. Images are 2 μm × 2 μm. Height scales are (methane, 40 °C) 230 nm; (methane, other) 40 nm; (nitrogen) 40 nm; (oxygen, 25 °C) 250 nm; and (oxygen, other) 40 nm.

dx.doi.org/10.1021/la2005387 |*Langmuir* 2011, 27, 8694–8699

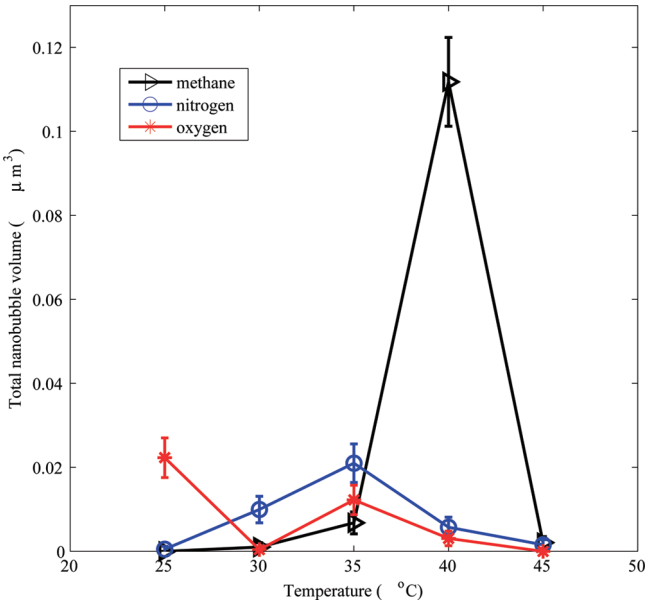

Figure 5. Total nanobubble volume on a 2 μm × 2 μm area as a function of gas type and temperature for methane (triangles), nitrogen (circles), and oxygen (asterisks). There is a clear maximum in density between 35 and 40 °C for all three gas types.

different temperatures on nucleation. For this, we repeated the experiments for methane, nitrogen, and oxygen, this time at system temperatures of 30, 35, 40, and 45 °C.

Typical images of nanobubbles created from the three gases, as functions of system temperature, are shown in Figure 4. It is evident that an optimal temperature exists for each type of gas that leads to maximum nanobubble nucleation. As an example, no nanobubbles nucleated from the methane-saturated water at 25 °C, but nucleation occurred for every temperature that we tested above this, with maximum production at 40 °C. These optimal temperatures are more clearly visible in the plots of the total nanobubble volume in Figure 5. Other work[17,35] has described a similar maximum in air-filled nanobubbles as being due to a maximum in solubility. However, if we compare the curves of Figure 5 to the temperature dependencies of the solubilities in Figure 1, it is clear that there is no corresponding peak in solubility (i.e. we reiterate that solubility is not the control parameter for nanobubble nucleation in gas-equilibrated systems).

In total, over 300 nanobubbles were imaged for the present study, so we have sufficient statistics to extract information for the contact angle versus the radius of curvature. We plot this for methane, nitrogen, and oxygen in Figure 6, where we use different symbols and colors to represent the differing system temperatures. For all of the gases in the present study, the contact angle was found to increase with increasing radius of curvature before leveling off to $\theta \rightarrow \sim 180°$ as $R \rightarrow \infty$.

When the contact angle is a function of the radius of curvature, it is necessary to introduce a line tension. Brenner and Lohse[10] suggest a functional form for this effect of

$$\cos\theta = \cos\theta_\infty - \frac{\cos\theta_\infty - \cos\theta_0}{1 + (R/\delta)} \qquad (1)$$

Here, θ_∞ is the value of the contact angle at large radii, θ_0 is at diminishingly small radii, and δ is the length scale over which we expect the line tension to take effect. Hence, we now choose to

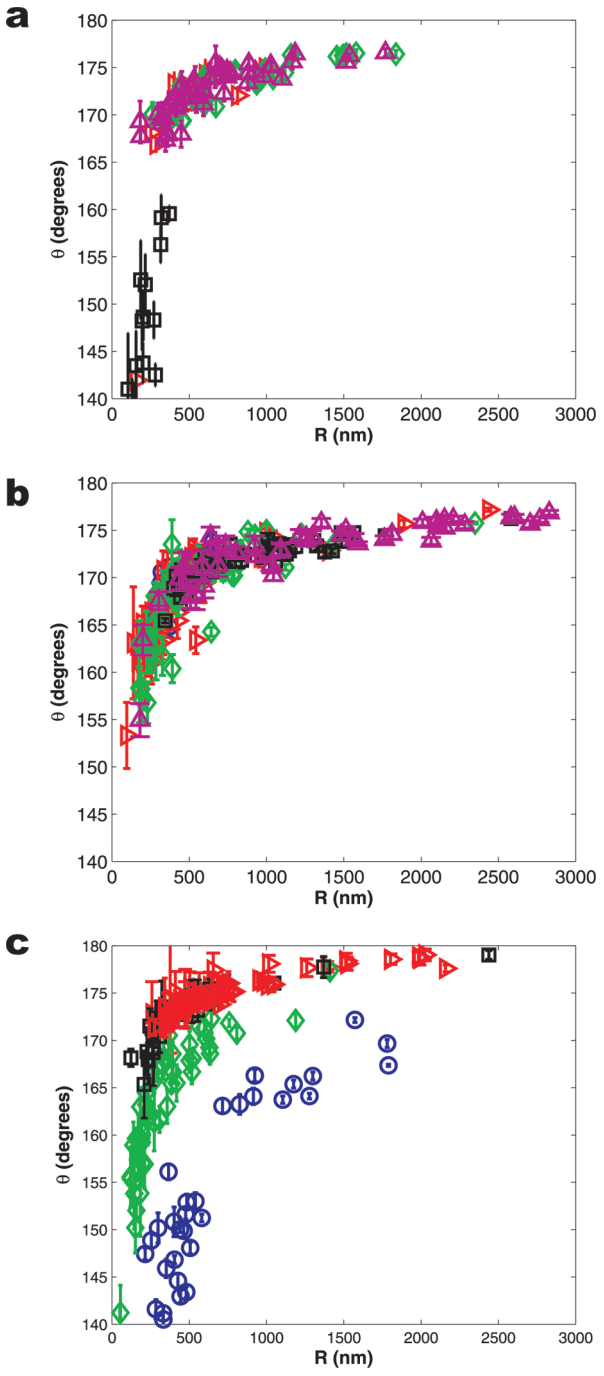

Figure 6. Contact angle as a function of the nanobubble radius of curvature for (a) methane, (b) nitrogen, and (c) oxygen nanobubbles at 25 (circles), 30 (right triangles), 35 (diamonds), 40 (squares), and 45 °C (up triangles). The dependence of the contact angle on the radius of curvature indicates that the line tension must be considered. The data have been corrected for cantilever tip distortion.

use the functional form of ref 10 for the nanoscale correction to the contact angle demonstrated in Figure 6. For the three fitting parameters θ_∞, θ_0, and δ, we set the two angles equal to 180 and 90° and use δ as the single fitting parameter for the data. These choices for the angles were selected because (i) it is clear from the data in Figure 6 that the contact angle tends to go to 180° with increasing radius of curvature and (ii) the contact angle rapidly

dx.doi.org/10.1021/la2005387 |*Langmuir* 2011, 27, 8694–8699

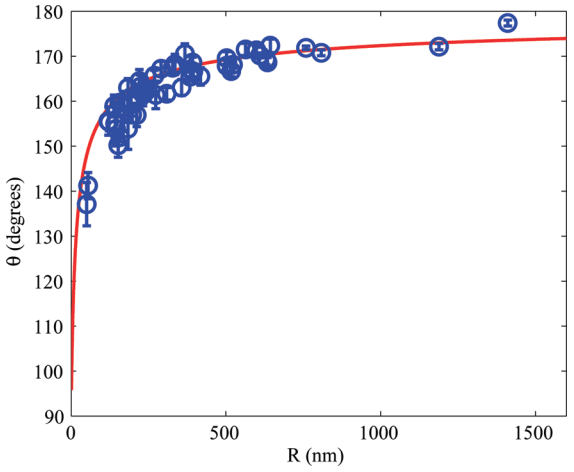

Figure 7. Fit of the 35 °C data for contact angle vs radius of curvature for oxygen. The fit is of the form $\cos\theta = \cos\theta_\infty - (\cos\theta_\infty - \cos\theta_0)/(1 + (R/\delta))$, with $\theta_\infty = 0°$, $\theta_0 = 90°$, and $\delta = 9$ nm. The corresponding line tension is $\tau = -\gamma\delta = -0.6$ nN.

decreases for smaller bubbles but we do not want or expect the nature of the material to change from hydrophobic to hydrophilic with decreasing radius of curvature. Within this framework, the line tension would be $\tau = -\gamma\delta$, where γ is the surface tension of water. A typical fit is shown in Figure 7, where we present the 35 °C data for oxygen. In this case, a line tension of $\tau \approx -0.6$ nN becomes important at a length scale of $\delta \approx 9$ nm.

Values of δ for each of the different gases used in this study as well as for the different temperatures used for methane, nitrogen, and oxygen are presented in Figure 8. There is a large spread in δ with gas type, which gives insight into the possible configuration of the nanobubble−substrate geometry. Different values of δ for different gas types means that the contact angle is different for different gas types. This is puzzling because the contact angle is dependent on the three differing surface energies of the three different interfaces (solid, liquid, and gas) but it is always the densest phase that contributes the most to these values. (As an example, degassing the air above the water level in a glass beaker does not lead to a change in the contact angle of the meniscus—the air has been evacuated, but the water and glass remain.) Thus, the specific type of gas should not have a noticeable effect on the contact angle because this is dominated by the water and solid. The way to resolve this issue of variable contact angle with gas type would be if the nanobubble was on top of a dense adsorbate ("micropancake"[43]) of gas molecules. As pointed out in ref 11, this is the most probable configuration for a nanobubble; if a nanobubble is on top of a dense adsorbate, then it is the binding energy of gaseous molecules to adsorbed molecules that should be considered, not the binding energy to the underlying solid. Not only does this explain the essentially constant value of the contact angle for air-filled nanobubbles, regardless of the substrate, but it also explains the difference in the contact angle with gas type. Of course, an underlying adsorbate would also provide a gas bank for the gaseous influx to balance the diffusive outflux in the dynamic equilibrium model of nanobubble stability.[10]

The mean value of the line tension here, which we calculate as the average of the data in Figure 8a,b, is $\tau \approx -0.8$ nN. The measurement of a negative line tension for nanobubbles/nanodroplets is expected.[44] Values in the literature include −3 nN,[27] ∼ −2.3 pN,[45] ∼ −0.2 nN,[21] and ∼ −1 pN.[44]

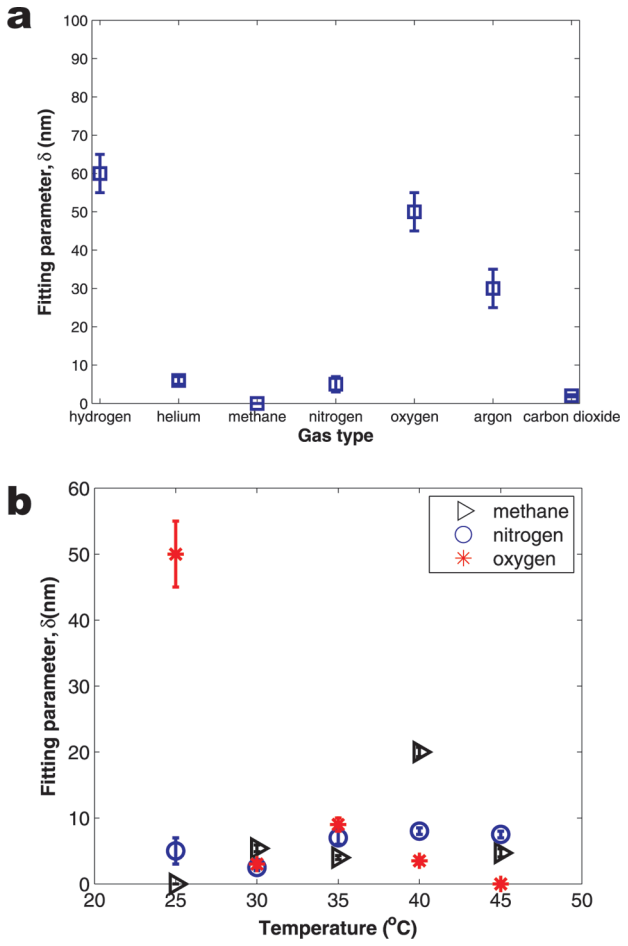

Figure 8. Fitting parameter δ (a) as a function of gas type at a temperature of 25 °C and (b) as a function of temperature for methane, nitrogen, and oxygen. The average line tension is $\tau = -\gamma\delta \approx -0.8$ nN.

Returning to Figure 8, we can again reiterate that we find no clear functional form linking the solubility or adsorption strength to different values of δ. Thus, we posit the following possible route to nucleation using the noble gases. Argon should adsorb more strongly to the substrate than helium, resulting in fewer argon nanobubbles, but the opposite is found. The fact that there is approximately an order of magnitude more argon available in the bulk, however, should increase the density of the adsorbate, possibly to include multiple layers. Thus, nanobubble nucleation may occur as a result of bulk desorption from the more weakly bound upper layers. For the diatomic molecules (hydrogen, nitrogen, and oxygen), it is much less clear. The strength of these adsorbates is dependent on the mean orientation of the molecules, and we would expect bulk desorption to occur much more readily than for the noble gases. The same is also true for the more complex molecules (carbon dioxide and methane).

CONCLUSIONS

We have shown that gas type is a key parameter in the nucleation of nanobubbles. Not only do specific gases lead to the formation of more nanobubbles than others, but there also exists an optimal temperature for nanobubble nucleation between ∼35 and ∼40 °C that appears to be weakly dependent on gas type.

Surprisingly, nanobubble nucleation is not directly dependent on either the solubility of the specific gas in water or the relative adsorption strength of the gas to the substrate. This indicates that nanobubbles do not form solely because of the amount of gas available in the bulk or from dense adsorbates (micropancakes) on the substrate. Furthermore, we should expect either zero or a very small dependence on the specific gas type for the gas-enrichment layer thickness near a hydrophobic substrate, so this does not provide an adequate solution to nucleation either.

Hence, nanobubble nucleation must come from a combination of several competing factors. Certainly, at least a two-stage nucleation process is most likely. More nanobubbles are found at increasing temperature for low temperatures, as would be consistent for systems reliant on desorption, whereas fewer nanobubbles are found at increasing temperature for high temperatures, now consistent with systems reliant on solubility. The crossover in behavior is at a temperature of ∼35−40 °C.

For all of the nanobubbles that we investigated, we found a dependence of the contact angle on the radius of curvature. We introduced a line-tension term of the form proposed by Brenner and Lohse.[10] On our PFDTS-coated silicon substrate, the average line tension was negative and equal to $\tau \approx -0.8$ nN.

AUTHOR INFORMATION

Corresponding Author
*E-mail: j.r.t.seddon@utwente.nl.

ACKNOWLEDGMENT

We acknowledge useful discussions with Detlef Lohse and Harold Zandvliet throughout this work. The research leading to these results has received funding from the European Community's Seventh Framework Programme (FP7/2007-2013) under grant agreement number 235873 and from the Foundation for Fundamental Research on Matter (FOM), which is sponsored by The Netherlands Organization for Scientific Research (NWO).

REFERENCES

(1) Parker, J. L.; Claesson, P. M.; Attard, P. *J. Phys. Chem.* **1994**, *98*, 8468–8480.
(2) Lou, S.-T.; Ouyang, Z.-Q.; Zhang, Y.; Li, X.-J.; Hu, J.; Li, M.-Q.; Yang, F.-J. *J. Vac. Sci. Technol., B* **2000**, *18*, 2573–2575.
(3) Tyrrell, J. W. G.; Attard, P. *Phys. Rev. Lett.* **2001**, *87*, 176104.
(4) Holmberg, M.; Kühle, A.; Garnaes, J.; Morch, K. A.; Boisen, A. *Langmuir* **2003**, *19*, 10510–10513.
(5) Steitz, R.; Gutberlet, T.; Hauss, T.; Klösgen, B.; Krastev, R.; Schemmel, S.; Simonsen, A. C.; Findenegg, G. H. *Langmuir* **2003**, *19*, 2409–2418.
(6) Simonsen, A. C.; Hansen, P. L.; Klösgen, B. *J. Colloid Interface Sci.* **2004**, *273*, 291–299.
(7) Zhang, X. H.; Zhang, X. D.; Lou, S. T.; Zhang, Z. X.; Sun, J. L.; Hu, J. *Langmuir* **2004**, *20*, 3813–3815.
(8) Borkent, B. M.; Dammer, S. M.; Schönherr, H.; Vancso, G. J.; Lohse, D. *Phys. Rev. Lett.* **2007**, *98*, 204502.
(9) Yang, S.; Kooij, E. S.; Poelsema, B.; Lohse, D.; Zandvliet, H. J. W. *Europhys. Lett.* **2008**, *81*, 64006.
(10) Brenner, M. P.; Lohse, D. *Phys. Rev. Lett.* **2008**, *101*, 214505.
(11) Seddon, J. R. T.; Lohse, D. *J. Phys.: Condens. Matter* **2011**, *23*, 133001.
(12) Zhang, X. H.; Quinn, A.; Ducker, W. A. *Langmuir* **2008**, *24*, 4756–4764.
(13) Ducker, W. A. *Langmuir* **2009**, *25*, 8907–8910.
(14) Seddon, J. R. T.; Zandvliet, H. J. W. *Surf. Sci.* **2010**, *604*, 476–477.
(15) Zhang, X. H.; Zhang, X.; Sun, J.; Zhang, Z.; Li, G.; Fang, H.; Xiao, X.; Zeng, X.; Hu, J. *Langmuir* **2007**, *23*, 1778–1783.
(16) Yang, S.; Dammer, S. M.; Bremond, N.; Zandvliet, H. J. W.; Kooij, E. S.; Lohse, D. *Langmuir* **2007**, *23*, 7072–7077.
(17) Seddon, J. R. T.; Kooij, E. S.; Poelsema, B.; Zandvliet, H. J. W.; Lohse, D. *Phys. Rev. Lett.* **2011**, *106*, 056101.
(18) Hampton, M. A.; Nguyen, A. V. *Adv. Colloid Interface Sci.* **2010**, *154*, 30–55.
(19) Although the authors of ref 6 present evidence of nanobubbles in pure alcohols, this has never been reproduced.
(20) Agrawal, A.; Park, J.; Ryu, D. Y.; Hammond, P. T.; Russell, T. P.; McKinley, G. H. *Nano Lett.* **2005**, *5*, 1751–1756.
(21) Kameda, N.; Nakabayashi, S. *Chem. Phys. Lett.* **2008**, *461*, 122–126.
(22) Borkent, B. M.; Schönherr, H.; Caër, G. L.; Dollet, B.; Lohse, D. *Phys. Rev. E* **2009**, *80*, 036315.
(23) Lou, S.; Gao, J.; Xiao, X.; Li, X.; Li, G.; Zhang, Y.; Li, M.; Sun, J.; Li, X.; Hu, J. *Mater. Charact.* **2002**, *48*, 211–214.
(24) Switkes, M.; Ruberti, J. W. *Appl. Phys. Lett.* **2004**, *84*, 4759–4761.
(25) Zhang, X. H.; Li, G.; Maeda, N.; Hu, J. *Langmuir* **2006**, *22*, 9238–9243.
(26) Kameda, N.; Sogoshi, N.; Nakabayashi, S. *Surf. Sci.* **2008**, *602*, 1579–1584.
(27) Yang, J.; Duan, J.; Fornasiero, D.; Ralston, J. *J. Phys. Chem. B* **2003**, *107*, 6139–6147.
(28) Miller, J. D.; Hu, Y.; Veeramasuneni, S.; Lu, Y. *Colloids Surf., A* **1999**, *154*, 137–147.
(29) Zhang, L.; Zhang, Y.; Zhang, X.; Li, Z.; Shen, G.; Ye, M.; Fan, C.; Fang, H.; Hu, J. *Langmuir* **2006**, *22*, 8109–8113.
(30) Yang, S.; Tsai, P.; Kooij, E. S.; Prosperetti, A.; Zandvliet, H. J. W.; Lohse, D. *Langmuir* **2009**, *25*, 1466–1474.
(31) Zhang, L.; Zhang, X.; Zhang, Y.; Hu, J.; Fang, H. *Soft Matter* **2010**, *6*, 4515–4519.
(32) Lide, D. R., Ed. *Handbook of Chemistry and Physics*, 86th ed.; Taylor and Francis: Boca Raton, FL, 2005.
(33) Rathgen, H. Superhydrophobic Surfaces: From Fluid Mechanics to Optics. Ph.D. Thesis, University of Twente, 2008.
(34) Seddon, J. R. T.; Bliznyuk, O.; Kooij, E. S.; Poelsema, B.; Zandvliet, H. J. W.; Lohse, D. *Langmuir* **2010**, *26*, 9640–9644.
(35) Zhang, X. H.; Li, G.; Wu, Z. H.; Zhang, X. D.; Hu, J. *Chin. Phys.* **2005**, *14*, 1774–1778.
(36) Dunne, J. A.; Mariwala, R.; Rao, M.; Sircar, S.; Gorte, R. J.; Myers, A. L. *Langmuir* **1996**, *12*, 5888–5895.
(37) Staudt, R.; Herbst, A.; Beutekamp, S.; Harting, P. *Adsorption* **2005**, *11*, 379–384.
(38) Sudik, A. C.; Millward, A. R.; Ockwig, N. W.; Cote, A. P.; Kim, J.; Yaghi, O. M. *J. Am. Chem. Soc.* **2005**, *127*, 7110–7118.
(39) Doshi, D. A.; Watkins, E. B.; Israelachvili, J. N.; Majewski, J. *Proc. Natl. Acad. Sci. U.S.A.* **2005**, *102*, 9458–9462.
(40) Dammer, S. M.; Lohse, D. *Phys. Rev. Lett.* **2006**, *96*, 206101.
(41) Mezger, M.; Reichert, H.; Schöder, S.; Okasinski, J.; Schröder, H.; Dosch, H.; Palms, D.; Ralston, J.; Honkimäki, V. *Proc. Nat. Acad. Sci. U.S.A.* **2006**, *103*, 18401–18404.
(42) Sendner, C.; Horinek, D.; Bocquet, L.; Netz, R. R. *Langmuir* **2009**, *25*, 10768–10781.
(43) Zhang, X. H.; Khan, A.; Ducker, W. A. *Phys. Rev. Lett.* **2007**, *98*, 136101.
(44) Weijs, J. H.; Marchand, A.; Andreotti, B.; Lohse, D.; Snoeijer, J. H. *Phys. Fluids* **2011**, *23*, 022001.
(45) Checco, A.; Guenoun, P.; Daillant, J. *Phys. Rev. Lett.* **2003**, *91*, 186101.